Temperature-Dependent Trap-Assisted Ultrafast Carrier Dynamics in Amorphous and Crystalline In$_2$Se$_3$ Thin Films

Palwinder Singh[1], Gurpreet Kaur,[1] Nandan Ghorai,[1] Tanmay Goswami,[1] Anup Thakur[2] and Hirendra N. Ghosh[1,3,*]

[1] *Institute of Nano Science and Technology, Mohali, Punjab 160062, India*

[2] *Advanced Materials Research Lab, Department of Basic and Applied Sciences, Punjabi University, Patiala, Punjab 147001, India*

[3] *Radiation and Photochemistry Division, Bhabha Atomic Research Centre, Mumbai 400085, India*

The presence of trap states plays an important role in the performance of optoelectronic devices. In the present investigation, charge-carrier dynamics in amorphous and crystalline In$_2$Se$_3$ thin films is studied using broadband femtosecond pump-probe spectroscopy in the temperature range of 5–300 K. Amorphous In$_2$Se$_3$ thin films (approximately 300 nm thick) are deposited using a thermal-evaporation method, and undergo a transition to a crystalline phase under vacuum annealing at 250 °C. Ultrafast transient absorption studies suggest that the charge-carrier dynamics is dominated by the presence of inter-band-gap defect states in both types of film, and it is found to be slower in the amorphous than in the crystalline material due to the presence of deep defect states in the amorphous material. The carrier dynamics in the amorphous film is faster at 5 K than at 300 K, as the probability of free carriers becoming trapped in defect states is much higher at high temperatures due to their higher mobility. The change in resistance under light and with temperature is directly correlated with ultrafast spectroscopic data.

I. INTRODUCTION

Two-dimensional (2D) materials exhibit interesting properties compared with their one- and three-dimensional counterparts. These materials have become a center of attraction among the scientific and industrial community in recent decades, due to their versatility in various fields [1,2]. Several alloys from the III-VI group have a van der Waals layered structure, and constitute an important class of semiconductors with tunable optical absorption from the ultraviolet to the near infrared. GaX, Ga$_2X_3$, InX, and In$_2X_3$ (X = S, Se, and Te), which are van der Waals layered 2D materials from the III-VI group, have been widely investigated for their application in photodetectors [3–7], field-effect transistors [8,9], terahertz detection [10], phase-change memories [11], second-harmonic generation [12], etc. Among these, In$_2$Se$_3$ exhibits interesting properties, *viz.* efficient exfoliation into individual layers with excellent structural and electronic properties, thickness-dependent optical properties [13], and high charge-carrier mobility [14]. In$_2$Se$_3$ has four stable phases (α, β, γ, and δ), among which the γ phase has a three-dimensional structure. The other phases have a layered structure, composed of five atomic layers Se-In-Se-In-Se, with strong covalent bonds within each quintuple layer and van der Waals interactions connecting neighboring quintuple layers [15]. A strong quantum confinement effect is observed in the optical properties of ultrathin α-In$_2$Se$_3$ [13].

The transition from an amorphous to a crystalline phase is the most important phenomenon exhibited by chalcogenide alloys. There is a noteworthy change in the optical and electrical properties associated with the phase transition. Studies of the carrier dynamics in both phases is crucial to enhancing the performance of materials for optoelectronic applications [16]. It is interesting to study the carrier dynamics in In$_2$Se$_3$ thin films in the amorphous and crystalline phases. There are few reports of the carrier dynamics in single crystals and nanoflakes of In$_2$Se$_3$ [16,17]. Tao *et al.* [16] investigated thickness-dependent recombination processes and found that α-In$_2$Se$_3$ shows bimolecular Auger recombination in thick layers and three-carrier Auger recombination in thin layers. However, there has been no systematic study of ultrafast carrier dynamics in phase-change materials in the literature. In addition to this, the effect of temperature on the carrier dynamics has never been reported.

In phase-change materials, different kinds of defect states exist that play an important role in the optical and electrical properties. Generally, these defect states are formed during the growth of crystals and the fabrication

*hnghosh@inst.ac.in

of thin films. An understanding of the mobility of charge carriers and the mechanism of their recombination through defects is a significant factor in designing optoelectronic devices. The carrier dynamics changes with the degree of disorder in the material. Generally, materials in the form of thin films contain more defects than do their nanocounterparts. Recently, Wang *et al.* [18] observed that both free and trapped carriers contribute to the photocurrent in solar cells. Zhao *et al.* [3] studied the mechanism of the photocurrent in InSe photodetectors via tailoring the density of trap states. Thus, it is important to know the location of trapped carriers and their relaxation pathways. In the present investigation, we synthesize amorphous In_2Se_3 thin films, where the amorphous $\longrightarrow$ crystalline phase transition is achieved by vacuum annealing, and monitor ultrafast charge-carrier dynamics in the temperature range of 5–300 K for both amorphous and crystalline films. Locations of the defect states in the forbidden band gap of amorphous and crystalline In_2Se_3 thin films are proposed on the basis of temperature-dependent ultrafast spectroscopic studies. The charge-carrier dynamics is also correlated with photoconductive measurements in different temperature ranges.

II. EXPERIMENTAL DETAILS

In the present research study, a bulk In_2Se_3 alloy is prepared by a melt-quenching technique [19,20] from a highly pure (99.999%) trace-metal basis of indium and selenium. Thin films of the synthesized In_2Se_3 alloy are deposited on glass substrates using a thermal-evaporation (HHV-BC-300) technique [19,20]. The thickness of the films is measured *in situ* by a digital thickness monitor (HHV DTM-101). The shutter is closed after a thickness of approximately 300 nm is achieved. The films are annealed at 150, 200, and 250 °C in a vacuum (approximately 10^{-3} mbar) for 2 h. Details of the other experimental techniques used can be found in the Supplemental Material [21].

To investigate the carrier dynamics further, ultrafast transient absorption measurements are performed using a Ti:sapphire amplifier system (Astrella, Coherent, 800 nm, 2-mJ pulse energy, 35-fs pulse width, and 1-kHz repetition rate) and a Helios Fire pump-probe spectrometer [22,23]. The desired excitation wavelength of the pump beam is selected from the output of an optical parametric amplifier (OPerA-SOLO). The probe beam is passed through a delay stage and is focused onto a sapphire crystal to generate white light pulses in the range of 420–780 nm. Ultrafast transient absorption measurements are performed at different temperatures (300, 150, 100, and 5 K) using a closed-cycle refrigerator (CRYO Industries, USA).

III. RESULTS AND DISCUSSION

The composition of the In_2Se_3 thin films is verified using an energy-dispersive x-ray spectroscopy technique,

and the atomic distribution is studied by elemental mapping; more information is presented in Fig. S1 in the Supplemental Material [21]. The deposited films are slightly rich in selenium. Figure 1(a) shows x-ray diffraction (XRD) patterns of an as-deposited In_2Se_3 thin film and films annealed at different temperatures (150, 200, and 250 °C) for 2 h. There is no sharp peak in the XRD patterns of the as-deposited thin film and the films annealed at 150 and 200 °C, which confirms the amorphous nature of the films. The XRD pattern of the In_2Se_3 thin film annealed at 250 °C confirms that it has a hexagonal structure [24] with space group $P6_3/mmc$.

The optical properties, including the band gap, absorption, and scattering coefficient, are among the most important aspects of these materials and are extremely important for their evaluation for optoelectronic applications. The transmission spectra of the as-deposited and annealed (150, 200, and 250 °C) In_2Se_3 thin films are shown in Fig. 1(b). All the films are highly transparent in the wavelength range of 680–2000 nm. Chalcogenide alloys are transparent beyond a wavelength of 1 μm, as these materials have high atomic masses, which generate low-energy phonons in the amorphous network, conferring wide optical transparency extending far into the near-infrared region. Here, it is interesting to observe that the crystalline In_2Se_3 is also
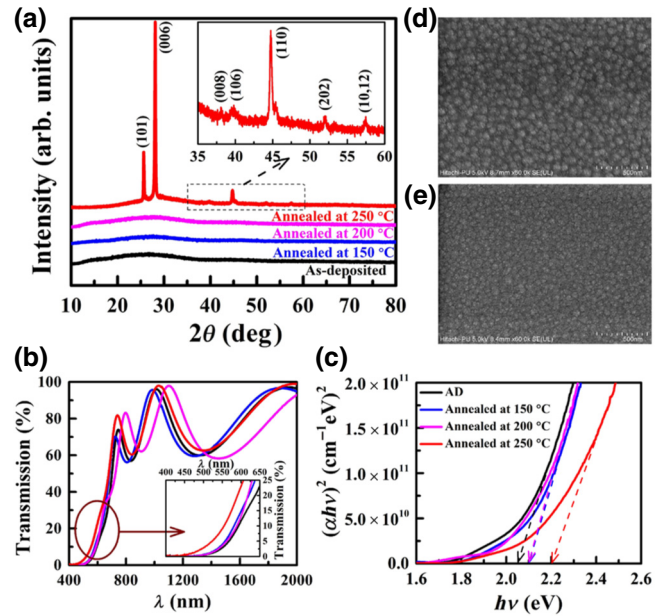

FIG. 1.   (a) XRD patterns of an as-deposited In_2Se_3 thin film and of films annealed at 150, 200, and 250 °C. (b) Transmission spectra of In_2Se_3 thin films: as-deposited (black), and annealed at 150 °C (blue), 200 °C (magenta), and 250 °C (red). The inset shows a magnified view of the absorption edge. (c) Relation between $(\alpha h\nu)^2$ and energy. The value of the intercept on the energy axis of the linear fit is the optical band gap. (d),(e) Field-emission-SEM images of In_2Se_3 thin films: (d) as-deposited, (e) annealed at 250 °C.

highly transparent beyond its absorption edge. There are transmission fringes in the regions of medium and weak absorption due to interference effects of light. The presence of these fringes implies uniform growth of the thin films. The positions of these fringes change with annealing because of a change in the refractive index of the material [25]. The change in the optical parameters associated with the phase transition is the basic mechanism that is used when chalcogenide alloys are employed in optical devices [26,27].

A blueshift in the absorption edge with annealing is observed, as shown in the inset of Fig. 1(b). This can be ascribed to a change in the optical band gap. The optical band gaps of all the films are calculated using Tauc's relation [28],

$$\alpha h\nu = \beta(h\nu - E_g)^n, \qquad (1)$$

where $h\nu$, β, and E_g denote the photon energy, band-tailing parameter, and optical band gap, respectively. The absorption coefficient (α) is an inherent property of the material and can be calculated using the relation

$$\alpha = \frac{1}{d}\ln\frac{1}{T}, \qquad (2)$$

where T is the optical transmission and d is the thickness of the film. The parameter n in Eq. (1) can have different values (1/2, 2, 3/2, and 3) depending upon the nature of the transition (direct allowed, indirect allowed, direct forbidden, and indirect forbidden, respectively). The relation between $(\alpha h\nu)^2$ and $h\nu$ is presented in Fig. 1(c). The optical band gaps of the as-deposited In_2Se_3 film and the film annealed at 250 °C are 2.06 and 2.20 eV, respectively. The optical band gap of the films annealed at 150 and 200 °C is 2.10 eV, which is marginally higher than the optical band gap of the as-deposited film, although all have an amorphous structure. This is due to a decrease in the local disorder in the film, which decreases the band tailing and increases the optical band gap with annealing at 150 and 200 °C.

The scattering of light from the surface of a thin film has a dependence on the microstructure of the crystallites [29]. The morphology of the as-deposited and 250 °C-annealed films is shown in Figs. 1(d) and 1(e). Uniform growth of these thin films is also observed in these figures. The cluster size is observed to decrease after the phase transition from the amorphous to the crystalline structure.

It can be clearly observed from our experimental results that there is a noteworthy change in the optical properties associated with the phase transition of the In_2Se_3 thin films. However, it is extremely important to monitor the charge-carrier dynamics in In_2Se_3 thin films, which includes the lifetime of the charge carriers together with their associated relaxation pathways, to find out about

their suitability for optoelectronic applications. To understand the carrier dynamics in amorphous and crystalline In_2Se_3 thin films, broadband femtosecond pump-probe spectroscopic measurements are carried out. The differential absorption (ΔA) records any change in the absorption spectrum as a function of time and wavelength. It is measured as the change in absorption of the probe after and before the pump ($\Delta A = A_{\text{pump on}}^{\text{probe}} - A_{\text{pump off}}^{\text{probe}}$). Differential absorption spectra of the amorphous and crystalline films are recorded after excitation with a 420-nm laser pulse [with a photon energy of 2.95 eV, which is higher than the optical band gap of both amorphous ($E_g = 2.06$ eV) and crystalline ($E_g = 2.20$ eV) In_2Se_3 thin films]. Photoexcitation of semiconductors with a photon energy higher than the band-gap energy generates charge carriers (electrons and holes) in the conduction and valence bands. The effective mass of holes in In_2Se_3 is approximately 5 times the mass of electrons, implying that the mobility of holes is far lower than that of electrons. This indicates that following photoexcitation, the major role is played by the electrons, since they are more mobile than the holes. Also, it has already been reported [16] that Auger bimolecular recombination processes dominate in thicker layers of In_2Se_3, of the kind that we are considering in our case, and so the excitonic recombination energy is transferred again to another exciton. In contrast, in the case of thinner layers, the Auger process is a three-body process, implying that the energy from excitonic recombination is transferred to holes, thus necessitating equal consideration of holes in the carrier dynamics (the Auger process imparts energy to the heavier carriers, owing to the smaller density of states in the corresponding band). However, it should be noted that the role of holes cannot be completely neglected here, and so the dynamics of the carriers as a whole (electrons and holes) is discussed in this paper, but it is worth noting that the electrons dominate the dynamics to a major extent.

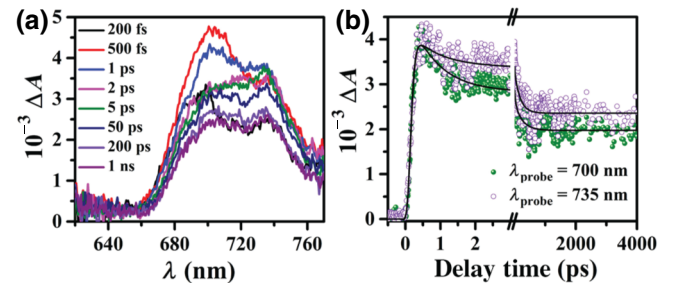Figure 2(a) shows the differential absorption spectra of the amorphous film after 420-nm excitation. The transient

FIG. 2. (a) Differential absorption spectra at different probe delays after laser excitation of an amorphous In_2Se_3 thin film at 420 nm at room temperature (300 K) with pulse energy 100 μJ/cm^2. (b) Normalized transient kinetic decay traces with probing at wavelengths of 700 and 735 nm.

TABLE I. Exponentially fitted parameters for the kinetics (with probing at 700 and 735 nm) of amorphous In_2Se_3 thin film at 300 K after excitation at 420 nm with an energy of 100 $\mu J/cm^2$.

λ_{probe} (nm)	Growth τ_g (fs)	Recovery		
		τ_1 (ps)	τ_2 (ps)	τ_3 (ns)
700	<100 (100%)	0.8 (34%)	29 (19%)	>1 (47%)
735	<100 (100%)	1.5 (13%)	50 (25%)	>1 (62%)

spectra show absorption in the range 660–770 nm, with a peak at 700 nm and a hump at 735 nm. The positive signal that appears in the transient absorption spectra of the amorphous film can be attributed to trapped charge carriers (both electrons and holes). It is intriguing to see that no transient bleaching is observed, due to the presence of defect states in the amorphous In_2Se_3 thin film. Interestingly, the transient signal at 700 nm decays faster than that at 735 nm on an early time scale. Transient signals are examined at wavelengths of both 700 and 735 nm to monitor the charge-carrier relaxation dynamics, and are shown in Fig. 2(b). The kinetic data can be fitted multiexponentially, and the fitting parameters are shown in Table I. The decay dynamics of the transient absorption can be attributed to the recombination dynamics of charge carriers (both electrons and holes) with different trap depths. The term "recovery" is used here merely to symbolize the system returning back to the equilibrium state, thus implying that whatever changes in the system are induced by the incident pump are slowly reversed through various relaxation mechanisms. This term can be applied to either the photoinduced absorption or the photobleaching signal returning back to the original $\Delta A = 0$ state, i.e., the unperturbed situation, indicating a sort of recovery to the initial conditions. So, it seems apt to use the terms "recovery" and "decay" interchangeably, since here they mean the development of the transient absorption signal with time, and are not intended to refer to some type of quasiparticle decay (e.g., the decay of an exciton over time).

The growth time for both wavelengths is found to be less than 100 fs (pulse-width limited). This indicates that prior to photoexcitation, the charge carriers populate defect states with different trap depths. The transient decay kinetics at 700 nm can be fitted multiexponentially with time constants $\tau_1 = 0.8$ ps (34%), $\tau_2 = 29$ ps (19%), and $\tau_3 > 1$ ns (47%). Here, the faster components (0.8 and 29 ps) can be assigned to the recombination dynamics of shallow trapped charge carriers [30]. The longer component (greater than 1 ns) can be attributed to the recombination dynamics of deep trapped carriers [30]. On the other hand, the transient kinetics at 735 nm can be fitted multiexponentially with time constants $\tau_1 = 1.5$ ps (13%), $\tau_2 = 50$ ps (25%), and $\tau_3 > 1$ ns (62%). The faster components (1.5 and 50 ps) can be assigned to the recombination dynamics

of shallow trapped charge carriers, and the longer component (greater than 1 ns) can be attributed to the recombination dynamics of deep trapped carriers. The transient kinetics at 700 nm is faster than that at 735 nm, suggesting that the majority of charge carriers are in a shallow trapped position for the 700-nm probe wavelength. As time progresses, the charge carriers are detrapped from the shallow states and make their way into deep trap sites on the way back to recombining with their counterparts. The carriers trapped in shallow states escape easily due to the availability of ample thermal energy at room temperature, but this is not the case with the deep trapped carriers, for which detrapping is difficult. It is also observed that there is a nonzero signal in the transient kinetics monitored at wavelengths of 700 and 750 nm after 4 ns. A long-lived signal similar to that in the present study has also been observed in other materials such as Sb_2Se_3, SnPb, and MoS_2 [18,31–33], due to the presence of such trap states. The charge-recombination dynamics is multiexponential and includes recombination of both hot and thermalized charge carriers and recombination of trapped charge carriers, including both shallow and deep trapped carriers. Finally, the signal intensity become zero as it reaches the equilibrium condition, which takes microseconds to less than a millisecond for these kinds of material.

It is clear from these ultrafast transient studies that localized states and defect states inside the band gap of the amorphous In_2Se_3 thin film play a major role in the charge-carrier dynamics. The presence of localized states and defect states in the forbidden gap of amorphous chalcogenide semiconductors has been discussed previously [34–36]. These states play an important role in defining the structural, electronic, and optical properties of amorphous chalcogenide semiconductors [37]. The origin of the localized states is the lack of long-range order and the presence of defect states inside the band gap. Generally, these defect states appear in chalcogenide alloys due to the presence of dangling bonds (wrong bonds), which are broken or unsatisfied bonds in a covalent solid, representing a type of point defect. The density of these unsatisfied bonds in amorphous semiconductors is very large (about 10^{18} cm^{-3}) [34].

To visualize the effect of crystallinity on the charge-carrier dynamics, we also carry out ultrafast transient absorption studies on a crystalline In_2Se_3 thin film after excitation at 420 nm, as shown in Fig. 3. Figure 3(a) shows the differential absorption spectra of the crystalline film at different time delays. It can be seen from the figure that the transient spectra of the crystalline film are completely different from those of the amorphous film [Fig. 2(a)]. New features in the differential absorption spectra of the crystalline film appear compared with the spectra of the amorphous film.

In the ultrafast transient spectra, with the structural transition from amorphous to crystalline, a photobleaching
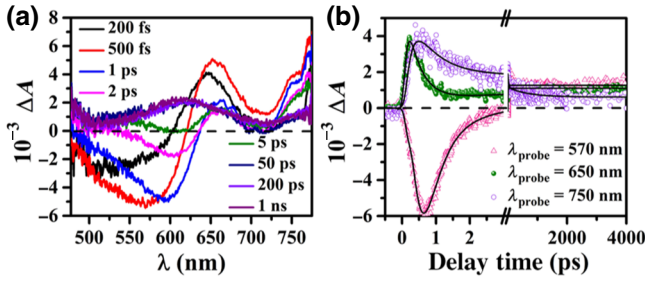
FIG. 3. (a) Differential absorption spectra at different probe delays after laser excitation of crystalline In_2Se_3 thin film at 420 nm at room temperature (300 K). (b) Normalized transient kinetic decay traces with probing at wavelengths of 570, 650, and 750 nm.

signal appears in the wavelength range of 480–620 nm, with a peak at approximately 540 nm, and two transient absorption bands in the 610–700 and 720–780-nm regions, peaking at 650 and 750 nm, respectively, on an early time scale (200 fs). The position of the bleaching matches well with the optical band gap of the crystalline film ($E_g = 2.20$ eV for the crystalline film, calculated from a Tauc plot). However, with time, the bleaching maximum moves into the red region of the spectrum, accompanied by narrowing of the full width at half maximum (FWHM) of the bleaching band (i.e., 100 nm at 200 fs and 58 nm at 2 ps). It is observed that the bleaching maximum shifts towards higher wavelength with increasing delay time of the probe pulse (i.e., 530 nm at 200 fs and 605 nm at 2 ps). This gradual redshift of the bleaching maximum can be attributed to the cooling dynamics of hot carriers in the conduction band of the crystalline In_2Se_3 thin film. The appearance of transient absorption bands at wavelengths of 650 and 750 nm is due to trap states. In polycrystalline films, these traps are mainly due to grain boundaries. The observed bleaching signal is not prominent, and becomes positive after 4.5 ps. It shows a derivativelike spectral feature due to carrier-induced spectral shifting, which is generally known as band-gap renormalization [18]. Similar behavior due to the indirect band gap of the material was also observed in an Sb_2Se_3 film [18]. In the present study, the long-term transient absorption is possibly due to the indirect optical band gap (approximately 2 eV) of elemental selenium, which may be present in the In_2Se_3. The fabricated

films are selenium rich, as verified by energy-dispersive-spectroscopy measurements [see the inset of Fig. S1(a) in the Supplemental Material [21]]. In earlier work [38,39], we have also observed positive absorption after 20 ps following the bleaching signal in CdTe/CdX ($X = $ S, Se) samples, and attributed this positive absorption to charge carriers trapped in different trap states. To understand the charge-carrier dynamics, the transient kinetics are monitored at 570, 650, and 750 nm, and are shown in Fig. 3(b). The kinetics are fitted multiexponentially, and the fitting parameters are listed in Table II.

It is interesting to see that the charge-carrier dynamics in the In_2Se_3 crystalline phase is drastically different from that in the amorphous phase. The appearance of a bleaching signal in the region of 570 nm clearly suggests a drastic reduction in the defect states in the crystalline phase. The bleaching signal originates when the pump laser pulse excites carriers from the valence band to the conduction band. As time passes, these carriers approach the bottom of the conduction band and the top of the valence band through relaxation processes; the time corresponding to this is the time of growth of the signal. After this, these carriers recombine either directly or through the process of trapping. The fastest time components of the recovery of the bleaching signal are attributed to the direct recombination of electrons at the bottom of the conduction band and holes at the top of the valence band. The next fast time component is attributed to recombination from shallow-level defects, and the longer-time component is due to recombination from deep traps. The bleaching can be fitted multiexponentially, with 130 fs of growth followed by recovery with $\tau_1 = 0.38$ ps (58%), $\tau_2 = 2.05$ ps (34%), $\tau_3 = 34$ ps (8%), and finally decay with $\tau > 1$ ns (−100%). Here, the 130-fs component of the bleaching signal can be attributed to the cooling time of carriers from hot states to the bottom of the conduction band and the top of the valence band; τ_1 is the fastest component and is related to direct recombination from the edges of the conduction and valence bands. It is interesting to note that this recombination accounts for more than 50% of the total bleaching. The fast recovery component (τ_2) is attributed to recombination through shallow defect levels and contributes the second highest recovery of the bleaching signal. Most of the bleaching signal (92%) is recovered with these two time constants. A negligible contribution

TABLE II. Exponentially fitted parameters for the kinetics (with probing at 570, 650, and 750 nm) of crystalline In_2Se_3 thin film at 300 K after excitation at 420 nm with an energy of 100 $\mu J/cm^2$.

| λ_{probe} (nm) | Growth | | Recovery | | | Decay |
	τ_g^1 (fs)	τ_g^2 (ps)	τ_1 (ps)	τ_2 (ps)	τ_3 (ps)	τ (ns)
570	130 (100%)	$\cdots$	0.38 (58%)	2.05 (34%)	34 (8%)	> 1 (−100%)
650	< 100 (92.5%)	2.8 (7.5%)	0.45 (75%)	$\cdots$	> 1000 (25%)	$\cdots$
750	110 (100 %)	$\cdots$	1.0 (65%)	75 (20 %)	> 1000 (15%)	$\cdots$

(from τ_3) to the bleaching recovery is made by recombination from deep traps due to elemental selenium in the In_2Se_3. The last decay component (τ) is attributed to achieving a state of equilibrium, which may take a longer time.

The transient positive absorption band at 650 nm can be fitted by a biexponential growth with time constants $\tau_g^1 < 100$ fs (92.5%) and $\tau_g^2 = 2.8$ ps (7.5%) and a biexponential decay with time constants $\tau_1 = 0.45$ ps (75%) and $\tau_2 > 1$ ns (25%). On the other hand, the transient band at 750 nm can be fitted by a single exponential growth with a time constant $\tau_g^1 = 110$ fs (100%) and a multiexponential decay with time constants $\tau_1 = 1$ ps (65%), $\tau_2 = 75$ ps (20%), and $\tau_3 > 1$ ns (15%). Although both of the transient bands at 650 and 750 nm indicate transient absorption due to trapped charge carriers, it is interesting to see that the kinetics are completely different at the two monitoring wavelengths, where both the growth and the decay dynamics are completely different. The growth components, *viz.* less than 100 fs at 650 nm and 110 fs at 750 nm, can be attributed to the cooling time of carriers from hot states in the conduction band to band-edge states. The first transient decay component, 0.45 ps (major component, 75%) at 650 nm and 1 ps (major component, 65%) at 750 nm, can be attributed to the charge recombination dynamics of shallow trapped carriers localized just below the band edge and deeper trapped carriers localized away from the band edge. It can be clearly seen that the electron recombination dynamics is much faster when the electrons are localized at shallow trap states than when they are in deep states. Here, the long components, greater than 1 ns at 650 and 750 nm, are due to the recombination dynamics of deep surface-state charge carriers. Similarly to the amorphous film, there is a nonzero signal for the crystalline film (but less than that for the amorphous film) in the transient kinetics monitored at wavelengths of 650 and 750 nm after 4 ns. In the amorphous film, there exist a large number of defect states, uniformly distributed and situated deeper in the forbidden region than those in the crystalline film.

In crystalline materials, the density of defect states is much less because of the restraints applied by the crystal structure. From the ultrafast transient absorption spectra and the kinetics, for both the amorphous and the crystalline thin films, the positions of the shallow (700 nm in the amorphous and 650 nm in the crystalline material) and the relatively deep defect states (735 nm in the amorphous and 750 nm in the crystalline material) can be located, since the transient positive absorption bands are due to trapped carriers (shallow and deep) inside the band gap. So, from the transient spectra, the relative locations of the defect states can be deduced for both the amorphous and the crystalline thin films. It is interesting to see that with the structural transition, not only does the defect density change, but also the energy levels of the defect states change in the band-gap region. In these

phase-change materials, phonons (representing vibrational excitations) play an important role in the carrier dynamics. The nature of the vibrational excitations is different in amorphous materials from that in crystalline ones, which affects the carrier-phonon interactions [40]. The density of defect states in the amorphous phase is significantly reduced on annealing at high temperature; this happens due to the phase transition. In ultrafast transient absorption studies, it has been observed that defect states play a major role in carrier dynamics. We realize that it is very important to understand the dynamics of charge carriers with decreasing film temperature (down to 5 K) for both the amorphous and the crystalline phase.

In the present investigation, we also carry out ultrafast transient absorption studies on amorphous and crystalline In_2Se_3 thin films at various temperatures (300, 150, 100, and 5 K) after exciting the samples at 420 nm with different time delays. Figure 4(a) shows the differential absorption spectra for the amorphous film at 5 K (results for other temperatures are shown in Fig. S2 in the Supplemental Material [21]). When the temperature is decreased from 300 to 5 K, changes in the amplitude and shape can be seen in the differential absorption spectra. It is interesting to see that the transient absorption spectra become broader, with a single broad peak, with a decrease in temperature from 300 to 5 K (Fig. 4(a) and Fig. S2 in the Supplemental Material [21]). The single broad peak may be due to overlapping peaks arising from defects lying so close together that their charge wave functions overlap. The presence of two peaks at 300 K may be ascribed to the presence of competing traps, which contribute to delayed recombination.

The kinetics at 700 and 735 nm (which corresponds to two humps in the differential absorption at 300 K) can be fitted multiexponentially; it includes pulse-width-limited growth (less than 100 fs) and multiexponential decay for both wavelengths. The fitting parameters are shown in Table III. The charge-carrier dynamics is very similar for both shallow and deep trapped charge carriers at 5 K (Table III), which is completely different from the situation at
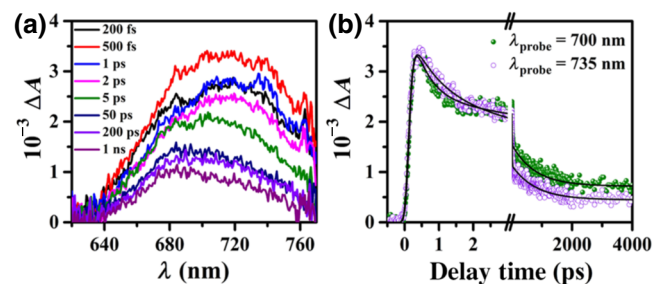

FIG. 4. (a) Differential absorption spectra at different probe delays after laser excitation of amorphous In_2Se_3 thin film at 420 nm at 5 K. (b) Normalized transient kinetic decay traces with probing at wavelengths of 700 and 735 nm.

TABLE III. Exponentially fitted parameters for the kinetics (with probing at 700 and 735 nm) of amorphous In_2Se_3 thin film at 5 K after excitation at 420 nm with an energy of 100 $\mu J/cm^2$.

λ_{probe} (nm)	Growth τ_g (fs)	Recovery		
		τ_1 (ps)	τ_2 (ps)	τ_3 (ns)
700	< 100 (100%)	0.48 (43%)	6 (24%)	> 1 (33%)
735	< 100 (100%)	0.55 (29%)	5 (42%)	> 1 (29%)

FIG. 5. (a) Differential absorption spectra at different probe delays after laser excitation of crystalline In_2Se_3 thin film at 420 nm at 5 K. (b) Normalized transient kinetic decay traces with probing at wavelengths of 570, 650, and 750 nm.

300 K (Table I). Tables I and III suggest that the charge-carrier recombination dynamics is much faster at 5 K than that at 300 K. As the film is cooled down to 5 K, the strength of lattice vibrations goes down, which ultimately reduces the carrier-phonon interaction. The effects of temperature can be compared for the first two components at 700 nm, as these decrease from 0.80 to 0.48 ps and from 29 to 6 ps with a decrease in temperature from 300 to 5 K in the amorphous film (Tables I and III). Generally, in ultrafast spectroscopy, the influence of carrier-phonon interaction can be seen on an early time scale (less than 2 ps). It has been widely reported in the literature that amorphous films have a large number of defect states. So, the probability of free carriers getting trapped in defect states is much higher at 300 K due to their higher mobility. Thus, a decrease in temperature from 300 to 5 K leads to a decrease in the mobility of free charge carriers, which consequently is responsible for faster recombination dynamics. The photoexcited charge carriers can recombine in both radiative and nonradiative ways. It has been reported in the literature that if the recombination process is dominated by nonradiative channels, the lifetime decreases with increasing temperature [30,41,42]. On the other hand, if the recombination process is dominated by radiative channels, the lifetime increases with increasing temperature. In the present investigation, it is observed that the carrier dynamics become faster in the amorphous film (Fig. S3 and Table S1 in the Supplemental Material [21]) with a decrease in temperature from 300 to 5 K. So, this clearly suggests that the recombination process on the early time scale may be radiative in nature. In that case, the long components should be attributed to a recombination process due to deep trapped carriers, which can give a long photoluminescence lifetime.

Figure 5(a) shows the transient spectra of the crystalline film at 5 K. Transient spectra at other temperatures are reported in the Supplemental Material [21]. The ultrafast transient spectra show transient bleaching in the 480–595-nm region, with a peak at approximately 540 nm and two transient absorption bands in the 600–710 and 730–780-nm regions, peaking at 650 and 750 nm, respectively, on an early time scale (200 fs). The bleaching maxima show a redshift accompanied by narrowing of the FWHM, i.e., 95 nm at 200 fs and 48 nm at 2 ps. To compare the carrier dynamics at temperatures of 300 and 5 K, the transient
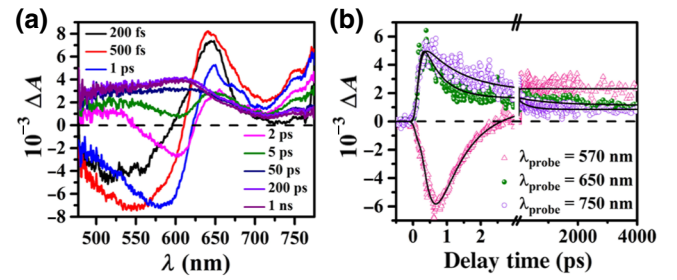
kinetics are again monitored at wavelengths of 570, 650, and 750 nm. Figure 5(b) depicts the transient kinetics at 570, 650, and 750 nm, and the fitting parameters of the kinetics are listed in Table IV.

The bleaching signal at 570 nm can be fitted multiex-ponentially, with 135 fs of growth followed by recovery with $\tau_1 = 0.45$ ps (49%), $\tau_2 = 2.45$ ps (41%), $\tau_3 = 4.50$ ps (4%), $\tau_4 = 37$ ps (6%), and finally a decay with a time constant greater than 1 ns (−100%). The growth component, 135 fs, of the bleaching signal can be attributed to the cooling time of carriers from hot states in the conduction and valence bands to band-edge states. The fastest recovery component, with a time constant of 0.45 ps, is attributed to direct recombination from the bottom of the conduction band to the top of the valence band. The fast recovery components 2.45 and 4.50 ps can be assigned to the charge-recombination dynamics of charge carriers from shallow trap depths. The fastest and fast components recover most (94%) of the bleaching signal. The slower component, with a time constant of 37 ps (6%), can be attributed to recombination from deep trap states, and, finally, the decay component with a time constant greater than 1 ns (τ) can be attributed to a return to the equilibrium state. The transient positive absorption band at 650 and 750 nm can be fitted by a single exponential growth with a time constant $\tau_g^1 < 100$ ps (100%). The transient decay kinetics at 650 nm can be fitted with time constants $\tau_1 = 0.57$ ps (78%), $\tau_2 = 50$ (4%), and $\tau_3 > 1$ ns (18%). On the other hand, the transient decay kinetics at 750 nm can be fitted with time constants $\tau_1 = 1.3$ ps (67%), $\tau_2 = 88$ ps (18%), and $\tau_3 > 1$ ns (15%). Although both of the transient bands at 650 and 750 nm are due to transient absorption due to trapped charge carriers, it is interesting to see that the kinetics are completely different at the two monitoring wavelengths. The growth component [less than 100 fs (100%)] at both 650 and 750 nm is pulse-width limited and can be attributed to the cooling time for carriers from hot states in the conduction band to band-edge states. The first transient decay component, 0.57 ps (major component, 78%) at 650 nm and 1.3 ps (major component,

TABLE IV.   Exponentially fitted parameters for the kinetics (with probing at 570, 650, and 750 nm) of crystalline In_2Se_3 thin film at 5 K after excitation at 420 nm with an energy of 100 $\mu J/cm^2$.

λ_{probe} (nm)	Growth τ_g^1 (fs)	Recovery				Decay τ (ns)
		τ_1 (ps)	τ_2 (ps)	τ_3 (ps)	τ_4 (ps)	
570	135 (100%)	0.45 (49%)	2.45 (41%)	4.5 (4%)	37 (6%)	> 1 (−100%)
650	< 100 (100%)	0.57 (78%)	50 (4%)	> 1000 (18%)	⋯	⋯
750	< 100 (100%)	1.3 (67%)	88 (18%)	> 1000 (15%)	⋯	⋯

67%) at 750 nm, can be attributed to the charge recombination dynamics of shallow trapped carriers localized just below the band edge and deeper trapped carriers localized away from the band edge. It can be clearly seen that the electron recombination dynamics is much faster when the electrons are localized at shallow trap states than when they are in deep states. Here, the long components with time constants greater than 1 ns at 650 and 750 nm are due to the recombination dynamics of deep surface-state charge carriers.

Unlike the case for the amorphous In_2Se_3 thin film, the carrier dynamics of the transient absorption bands at both 650 and 750 nm for the crystalline film are not similar at 5 K (Table IV). The growth component of the bleaching is found to be increased by 5 fs, and that of the transient bands at 750 nm by 10 fs. The slight increase in the growth component is due to strong carrier-phonon interaction at lower temperatures compared with 300 K. The recovery of the bleaching and of the transient absorption bands at both 650 and 750 nm is slower at 5 K (Tables II and IV). The recovery of the transient absorption bands at 650 and 750 nm for the crystalline film is different at 5 K from that at 300 K (Tables II and IV). The contributions of the longer component (greater than 1 ns) of the transient absorption band at 750 nm at 300 and 5 K are similar. On the other hand, the contribution of the longer component of the transient absorption band at 650 nm is 25% at 300 K and 18% at 5 K, which could be due to the density of deep defect states being at its minimum at 5 K.

Further, to understand the effect of trap states in the amorphous and crystalline In_2Se_3 thin films, electrical measurements over a temperature range from 80 to 700 K in darkness and under light (wavelength 405 nm with intensity 80 mW) are performed. The sheet resistance (R_s) is calculated using the van der Pauw formula,

$$R_s = \frac{\pi R}{\ln 2}. \tag{3}$$

Here, R is the reciprocal of the slope of the *I-V* curve and is measured in megaohms. Figure 6 shows the variation of the sheet resistance with temperature for amorphous and crystalline In_2Se_3 thin films. The sheet resistance of both films decreases with increasing temperature, and there is a further decrease under light. The electrical transport is based

on different phenomena in different temperature regimes in chalcogenide semiconductors. The sheet resistance of the amorphous In_2Se_3 thin film in the dark drops by 3 orders of magnitude in the temperature range of 80–300 K and by 2 orders of magnitude in the temperature range of 550–700 K. On the other hand, the sheet resistance of the crystalline In_2Se_3 thin film in the dark drops by 2 orders of magnitude in the temperature range of 80–300 K, 1 order of magnitude in the temperature range of 350–500 K, and another 1 order of magnitude in the temperature range of 550–700 K. It is interesting to note that there is a drop of 7 orders of magnitude from 80 to 700 K for the as-deposited film and a drop of 5 orders of magnitude from 80 to 700 K for the annealed film. At higher temperatures, thermal energy is the dominant factor that excites carriers, while light energy is solely responsible for the excitation of carriers at lower temperatures, and so the major effect of light can be seen in the temperature range of 80–300 K [as shown in the insets of Figs. 6(a) and 6(b)].

Carrier generation and recombination at different temperatures are affected by the presence of trap states [43]. At low temperatures, where less energy is available to excite carriers into the bands, localized carriers play a role in the transport mechanism through a hopping process [44]. There is a large contrast in the sheet resistance at 80 K compared with 300 K under conditions of light off and light on for the crystalline film, unlike the case for the amorphous film, as shown in the insets of Figs. 6(a) and 6(b). But this contrast is greater at 80 K for both samples. This behavior in the sheet resistance can be correlated with
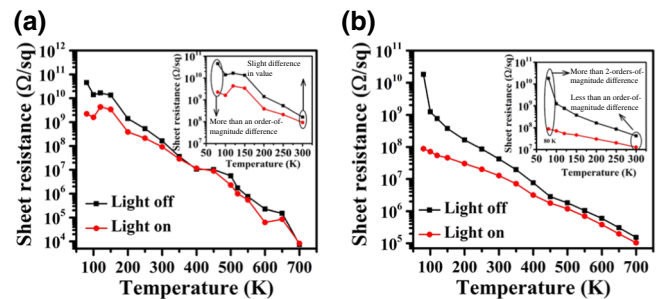

FIG. 6.   Variation of sheet resistance with temperature under conditions of light off and light on: (a) amorphous In_2Se_3 thin film and (b) crystalline In_2Se_3 thin film.

our femtosecond transient data. We observe that the density of trap states is greater in the amorphous phase and that the carrier dynamics is different at different temperatures. There is quenching of the lattice vibrations with a decrease in temperature, which further changes the carrier dynamics (Tables I and III). On the other hand, there is a smaller number of trap states in the crystalline film, and so less scattering of free carriers occurs through these traps, which ultimately increases the photoconductivity at lower temperature under light.

Crystalline materials are always preferable candidates for optoelectronic devices because of the smaller number of defect states, as it is believed that trap states reduce the performance of devices. The carrier dynamics plays a vital role in predicting the applicability of amorphous materials in optoelectronic devices. Temperature-dependent ultrafast transient studies and photoconductivity measurements give direct proof that defect states reduce the mobility of charge carriers and can be counterproductive in any device fabrication process.

IV. CONCLUSIONS

Amorphous In_2Se_3 thin films are deposited, and a structural transition from an amorphous to a crystalline phase is achieved by vacuum annealing at $250\,^\circ C$. Ultrafast charge-carrier dynamics in photoexcited In_2Se_3 thin films is monitored with the aid of femtosecond broadband pump-probe spectroscopy in the temperature range of 5–300 K. The charge recombination dynamics are found to be slower in the amorphous In_2Se_3 thin films due to the presence of a higher density of defect states inside the band gap. Temperature-dependent measurements suggest that the carrier recombination dynamics is much faster at 5 K than at 300 K in an amorphous film; however, not much difference is observed in a crystalline film. Here, in the amorphous film, the probability of free carriers becoming trapped in defect states is much higher at high temperatures due to their higher mobility. A direct correlation between the charge-carrier dynamics and the photoconductivity with varying temperature is established, which suggests that defect states play a major role in reducing the mobility of charge carriers and are a fundamental factor to be considered in device fabrication.

[1] Z. Lin, Y. Huang, and X. Duan, Van der Waals thin-film electronics, Nat. Electron. **2**, 378 (2019).

[2] T. Yu, H. Nie, S. Wang, B. Zhang, S. Zhao, Z. Wang, J. Qiao, B. Han, J. He, and X. Tao, Two-dimensional GeP-based broad-band optical switches and photodetectors, Adv. Opt. Mater. **8**, 1901490 (2019).

[3] Q. Zhao, W. Wang, F. Carrascoso-Plana, W. Jie, T. Wang, A. Castellanos-Gomez, and R. Frisenda, The role of traps in the photocurrent generation mechanism in thin InSe photodetectors, Mater. Horiz. **7**, 252 (2020).

[4] W. Feng, Z. Jin, J. Yuan, J. Zhang, S. Jia, L. Dong, J. Yoon, L. Zhou, R. Vajtai, J. M. Tour *et al.*, A fast and zero-biased photodetector based on GaTe–InSe vertical 2D p–n heterojunction, 2D Mater. **5**, 025008 (2018).

[5] Y. X. Fang, H. Zhang, F. Azad, S. P. Wang, F. C. C. Ling, and S. C. Su, Band offset and an ultra-fast response UV-VIS photodetector in γ-In_2Se_3/p-Si heterojunction heterostructures, RSC Adv. **8**, 29555 (2018).

[6] S. Chen, X. Liu, X. Qiao, X. Wan, K. Shehzad, X. Zhang, Y. Xu, and X. Fan, Facile synthesis of γ-In_2Se_3 nanoflowers toward high performance self-powered broadband γ-In_2Se_3/Si heterojunction photodiode, Small **13**, 1604033 (2017).

[7] N. Balakrishnan, C. R. Staddon, E. F. Smith, J. Stec, D. Gay, G. W. Mudd, O. Makarovsky, Z. R. Kudrynskyi, Z. D. Kovalyuk, L. Eaves *et al.*, Quantum confinement and photoresponsivity of β-In_2Se_3 nanosheets grown by physical vapour transport, 2D Mater. **3**, 025030 (2016).

[8] Y. H. Chen, C. Y. Cheng, S. Y. Chen, J. S. D. Rodriguez, H. T. Liao, K. Watanabe, T. Taniguchi, C. W. Chen, R. Sankar, F. C. Chou *et al.*, Oxidized-monolayer tunneling barrier for strong fermi-level depinning in layered InSe transistors, npj 2D Mater. Appl. **3**, 1 (2019).

[9] V. K. Sangwan, J. Kang, and M. C. Hersam, Thickness-dependent charge transport in exfoliated indium selenide vertical field-effect transistors, Appl. Phys. Lett. **115**, 243104 (2019).

[10] S. Mou, A. Rubano, and D. Paparo, Terahertz hyper-raman time-domain spectroscopy of gallium selenide and its application in terahertz detection, Appl. Phys. Lett. **115**, 211105 (2019).

[11] B. Yu, S. Ju, X. Sun, G. Ng, T. D. Nguyen, M. Meyyappan, and D. B. Janes, Indium selenide nanowire phase-change memory, Appl. Phys. Lett. **91**, 133119 (2007).

[12] J. Zhou, J. Shi, Q. Zeng, Y. Chen, L. Niu, F. Liu, T. Yu, K. Suenaga, X. Liu, J. Lin *et al.*, InSe monolayer: Synthesis, structure and ultra-high second-harmonic generation, 2D Mater. **5**, 025019 (2018).

[13] J. Quereda, R. Biele, G. Rubio-Bollinger, N. Agraït, R. D'Agosta, and A. Castellanos-Gomez, Strong quantum confinement effect in the optical properties of ultrathin α-In_2Se_3, Adv. Opt. Mater. **4**, 1939 (2016).

[14] D. A. Bandurin, A. V. Tyurnina, L. Y. Geliang, A. Mishchenko, V. Zólyomi, S. V. Morozov, R. K. Kumar, R. V. Gorbachev, Z. R. Kudrynskyi, S. Pezzini *et al.*, High electron mobility, quantum Hall effect and anomalous optical response in atomically thin InSe, Nat. Nanotechnol. **12**, 223 (2017).

[15] W. Li, F. P. Sabino, F. C. de Lima, T. Wang, R. H. Miwa, and A. Janotti, Large disparity between optical and fundamental

band gaps in layered In$_2$Se$_3$, Phys. Rev. B **98,** 165134 (2018).

[16] X. Tao, E. Mafi, and Y. Gu, Ultrafast carrier dynamics in single-crystal In$_2$Se$_3$ thin layers, Appl. Phys. Lett. **103,** 193115 (2013).

[17] R. Wang, T. Wang, Y. Zhou, Y. Wu, X. Zhang, X. He, H. Peng, J. Zhao, and X. Qiu, Layer-dependent ultrafast dynamics of α-In$_2$Se$_3$ nanoflakes, 2D Mater. **6,** 035034 (2019).

[18] K. Wang, C. Chen, H. Liao, S. Wang, J. Tang, M. C. Beard, and Y. Yang, Both free and trapped carriers contribute to photocurrent of Sb$_2$Se$_3$ solar cells, J. Phys. Chem. Lett. **10,** 4881 (2019).

[19] P. Singh, A. P. Singh, J. Sharma, A. Kumar, M. Mishra, G. Gupta, and A. Thakur, Reduction of Rocksalt Phase in Ag-Doped Ge$_2$Sb$_2$Te$_5$: A Potential Material for Reversible Near-Infrared Window, Phys. Rev. Appl. **10,** 054070 (2018).

[20] R. Kaur, P. Singh, K. Singh, A. Kumar, and A. Thakur, Optical band gap tuning of Sb-Se thin films for xerographic based applications, Superlattices Microstruct. **98,** 187 (2016).

[21] See Supplemental Material at http://link.aps.org/supplemental/10.1103/PhysRevApplied.14.014087 for experimental details and additional data.

[22] G. Kaur, K. Justice Babu, N. Ghorai, T. Goswami, S. Maiti, and H. N. Ghosh, Polaron-mediated slow carrier cooling in a type-1 3D/0D CsPbBr$_3$@Cs$_4$PbBr$_6$ core–shell perovskite system, J. Phys. Chem. Lett. **10,** 5302 (2019).

[23] S. Mondal, R. Aepuru, J. Dana, N. Ghorai, and H. N. Ghosh, Biexciton dissociation dynamics in nanohybrid Au–CuInS$_2$ nanocrystals, J. Phys. Chem. C **122,** 28497 (2018).

[24] S. Popović, A. Tonejc, B. Gržeta-Plenković, B. Čelustka, and R. Trojko, Revised and new crystal data for indium selenides, J. Appl. Crystallogr. **12,** 416 (1979).

[25] P. Singh, P. Sharma, V. Sharma, and A. Thakur, Linear and non-linear optical properties of Ag-doped Ge$_2$Sb$_2$Te$_5$ thin films estimated by single transmission spectra, Semicond. Sci. Tech. **32,** 045015 (2017).

[26] P. Singh, A. P. Singh, N. Kanda, M. Mishra, G. Gupta, and A. Thakur, High transmittance contrast in amorphous to hexagonal phase of Ge$_2$Sb$_2$Te$_5$: Reversible NIR-window, Appl. Phys. Lett. **111,** 261102 (2017).

[27] K. Shportko, S. Kremers, M. Woda, D. Lencer, J. Robertson, and M. Wuttig, Resonant bonding in crystalline phase-change materials, Nat. Mater. **7,** 653 (2008).

[28] J. Tauc, Optical properties and electronic structure of amorphous Ge and Si, Mater. Res. Bull. **3,** 37 (1968).

[29] E. S. P. Leong, Y. J. Liu, B. Wang, and J. Teng, Effect of surface morphology on the optical properties in metal-dielectric-metal thin film systems, ACS Appl. Mater. Interfaces **3,** 1148 (2011).

[30] Z. Urgessa, J. Botha, M. O. Eriksson, C. Mbulanga, S. Dobson, S. Tankio Djiokap, K. F. Karlsson, V. Khranovskyy,

R. Yakimova, and P.-O. Holtz, Low temperature near band edge recombination dynamics in ZnO nanorods, J. Appl. Phys. **116,** 123506 (2014).

[31] J. Tong, Z. Song, D. H. Kim, X. Chen, C. Chen, A. F. Palmstrom, P. F. Ndione, M. O. Reese, S. P. Dunfield, O. G. Reid *et al.*, Carrier lifetimes of >1 μs in Sn-Pb perovskites enable efficient all-perovskite tandem solar cells, Science **364,** 475 (2019).

[32] X. Liu, X. Xiao, Y. Yang, D.-J. Xue, D.-B. Li, C. Chen, S. Lu, L. Gao, Y. He, M. C. Beard *et al.*, Enhanced Sb$_2$Se$_3$ solar cell performance through theory-guided defect control, Prog. Photovolt. **25,** 861 (2017).

[33] H. Shi, R. Yan, S. Bertolazzi, J. Brivio, B. Gao, A. Kis, D. Jena, H. G. Xing, and L. Huang, Exciton dynamics in suspended monolayer and few-layer MoS$_2$ 2D crystals, ACS Nano **7,** 1072 (2013).

[34] N. F. Mott, E. A. Davis, and R. A. Street, States in the gap and recombination in amorphous semiconductors, Philos. Mag. **32,** 961 (1975).

[35] M. H. Cohen, H. Fritzsche, and S. R. Ovshinsky, Simple Band Model for Amorphous Semiconducting Alloys, Phys. Rev. Lett. **22,** 1065 (1969).

[36] E. A. Davis and N. F. Mott, Conduction in non-crystalline systems V. Conductivity, optical absorption and photoconductivity in amorphous semiconductors, Philos. Mag. **22,** 0903 (1970).

[37] S. R. Elliott, *Physics of Amorphous Materials* (Longman, New York, 1984).

[38] S. Rawalekar, S. Kaniyankandy, S. Verma, and H. N. Ghosh, Surface-state-mediated charge-transfer dynamics in CdTe/CdSe core–shell quantum dots, Chem. Phys. Chem **12,** 1729 (2011).

[39] S. Rawalekar, S. Kaniyankandy, S. Verma, and H. N. Ghosh, Ultrafast charge carrier relaxation and charge transfer dynamics of CdTe/CdS core-shell quantum dots as studied by femtosecond transient absorption spectroscopy, J. Phys. Chem. C **114,** 1460 (2010).

[40] M. F. Thorpe and L. Tichý, *Properties and Applications of Amorphous Materials* (Springer, Netherlands, 2001), Vol. 9.

[41] I. Robin, B. Gauron, P. Ferret, C. Tavares, G. Feuillet, L. S. Dang, B. Gayral, and J. Gérard, Evidence for low density of nonradiative defects in ZnO nanowires grown by metal organic vapor-phase epitaxy, Appl. Phys. Lett. **91,** 143120 (2007).

[42] L. L. Yang, Q. Zhao, M. Q. Israr, J. R. Sadaf, M. Willander, G. Pozina, and J. Yang, Indirect optical transition due to surface band bending in ZnO nanotubes, J. Appl. Phys. **108,** 103513 (2010).

[43] Z. M. Liao, C. Hou, L. P. Liu, and D. P. Yu, Temperature dependence of photoelectrical properties of single selenium nanowires, Nanoscale Res. Lett. **5,** 926 (2010).

[44] D. Krebs, T. Bachmann, P. Jonnalagadda, L. Dellmann, and S. Raoux, Changes in electrical transport and density of states of phase change materials upon resistance drift, New J. Phys. **16,** 043015 (2014).